Engineering Transactions, **74**(1): 3–17, 2026, https://doi.org/10.24423/engtrans.2026.3488
Institute of Fundamental Technological Research Polish Academy of Sciences (IPPT PAN)
Université de Lorraine • Poznan University of Technology

Research Paper

Changes in the Damping Ratio and Energy Transfer Ratio Due to Damage in a Composite Beam

Małgorzata Jarosińska

Faculty of Civil and Environmental Engineering,
West Pomeranian University of Technology in Szczecin
Szczecin, Poland

e-mail: jarosinska@zut.edu.pl

This paper investigates changes in the modal parameters of a composite beam resulting from damage introduced to the bottom flange of a steel I-beam. Variations in the modal damping ratio and energy transfer ratio (ETR) are analysed. The results of experimental tests and numerical analyses are presented. The beam was modelled using the rigid finite elements (RFEs) method. The introduced damage caused small changes in the damping ratio. In contrast, the ETR was found to be more sensitive to damage than the damping ratio in the experimental results, exhibiting variations on the order of several tens of percent. In the numerical simulation results, changes in the ETR were smaller, reaching a few percent.

Keywords: steel-concrete composite beam, damage detection, energy transfer ratio (ETR).

1. Introduction

The use of composite structures is a solution increasingly chosen by engineers. The most common form of composite structure used in construction is the steel-concrete system. Steel-concrete composite structures use the compressive strength of concrete and the tensile strength of steel, resulting in an efficient and lightweight structure. Interaction between concrete and steel is made possible by a shear connector welded to the steel beam. Thus, with suitable connection between the concrete slab and the steel beam, slip between the two materials is eliminated. This increases stiffness and strength of such a composite element. In bridge structures, composite elements are readily used due to their favourable functional properties and economic considerations. In the literature, one can find papers in which researchers present solutions for innovative composite structures such as hybrid girders [1–3] or girders with corrugated steel webs [4, 5]. Often,

however, the most reasonable solution turns out to be the use of classic composite beams. Steel-concrete composite beams are used in bridges as well as in multi-storey buildings. Such beams may incorporate different types of connectors such as welded headed studs, perfobond connectors, angle and channel connectors, and many others [6].

It should be noted that in a dynamic industry and increased transport, ensuring the safety of bridge structures during day-to-day use plays a key role. Throughout their service life structures incur damage due to environmental and/or human factors. This is why it is important to use structural health monitoring (SHM) systems that allow the condition of the structure to be monitored in real time. The topic of SHM has been taken up by researchers for many years [7–10]. Changes in the dynamic response of a system can be a valuable tool used for detecting damage occurring in a structure.

The energy transfer ratio (ETR) was proposed by Liang and Lee [11]. It determines the ratio of modal energy transferred during a cycle to the total modal energy stored in the structure before that cycle. The energy transferred between vibration modes exists for non-proportionally damped systems, i.e., in systems where the proportional damping relationship given by Caughey and O'Kelly [12] is not satisfied:

$$\mathbf{C}\mathbf{M}^{-1}\mathbf{K} = \mathbf{K}\mathbf{M}^{-1}\mathbf{C}, \tag{1.1}$$

where $\mathbf{M}$, $\mathbf{C}$, $\mathbf{K}$ are the mass, damping, and stiffness matrices, respectively.

It should be noted that proportional damping is often used in practice because it is the simplest damping model, but it cannot be applied to many real-world structures. In fact, engineering structures belong to non-proportional systems. For such systems, the mode shapes are complex [13, 14]. Complex mode shapes are vectors that represent vibrations whose points do not pass through their equilibrium positions at the same time. This means that successive points reach their maximum excursions at different times – they have different phases. A complex mode shape is described by a real part and an imaginary part or, by introducing polar coordinates, by amplitude and phase. For such a system, there is a certain amount of energy transferred between the mode shapes and ETR $\neq 0$. Many previous works have confirmed that the energy transfer ratio is sensitive to damage. Studies conducted for steel-concrete bridge models with damage, such as bearing damage and girder damage, in which ETR was analysed, can be found in [15–17]. In addition, it should be mentioned here that the ETR can be determined globally (for the entire system under analysis) and locally (for individual regions of the system).

Previous studies carried out on damage diagnostics in composite beams have shown that changes in ETR as a result of damage are greater than changes in other modal parameters, such as natural frequency or damping ratio. In [18], the

authors presented the results of numerical analyses for a beam with composite damage at one of its ends. In [19], also based on numerical studies, a composite beam with different types of damage was investigated: (1) damage to the composite but in a different location than before, (2) damage to the concrete slab, and (3) simultaneous damage to the composite and the concrete slab. In a subsequent paper [20], the analysis of the composite damage of a beam was presented both in terms of numerical and experimental tests.

The work presented here is a continuation of the analyses of the sensitivity of ETR to damage in a steel-concrete composite beam. Earlier studies were carried out for other beams and a different type of damage. The choice of the present damage type was dictated by the desire to see how the parameters characterising damping behave as a result of damage to the steel part of the composite beam. Results are presented both for numerical analyses and experimental tests. The analysed beam had previously been tested for changes in natural frequencies and curvature of the mode shape [21]. In this study, the focus is on assessing the sensitivity of the damping ratio and the ETR to damage to the I-beam of the beam. The paper presents the results of the analyses for a globally determined ETR, that is, for the whole beam. As a multi-material system, the composite beam is not proportionally damped. This is due to the fact that steel, concrete and connectors have different damping properties. For such systems, there is an energy transfer between the vibration modes. The parameter that describes this phenomenon is defined as the ETR and is analysed in this paper.

2. Theoretical basis of the ETR

The homogeneous equation of motion for an n-DOF is as follows:

$$\mathbf{M}\ddot{\mathbf{X}} + \mathbf{C}\dot{\mathbf{X}} + \mathbf{K}\mathbf{X} = \mathbf{0}, \tag{2.1}$$

where $\mathbf{M}$, $\mathbf{C}$, $\mathbf{K}$ are the mass, damping, and stiffness matrices $(n \times n)$, and $\ddot{\mathbf{X}}$, $\dot{\mathbf{X}}$, $\mathbf{X}$ are the acceleration, velocity, and displacement vectors $(n \times 1)$, respectively.

Equation (2.1) can also be written in a modified form:

$$\ddot{\mathbf{Y}} + \overline{\mathbf{C}}\dot{\mathbf{Y}} + \overline{\mathbf{K}}\mathbf{Y} = \mathbf{0}, \tag{2.2}$$

where $\mathbf{Y} = \mathbf{M}^{0.5}\mathbf{X}$. The matrices $\overline{\mathbf{C}}$ and $\overline{\mathbf{K}}$ are the damping and stiffness matrices, respectively, defined as $\overline{\mathbf{C}} = \mathbf{M}^{-0.5}\mathbf{C}\mathbf{M}^{-0.5}$ and $\overline{\mathbf{K}} = \mathbf{M}^{-0.5}\mathbf{K}\mathbf{M}^{-0.5}$. For the modified stiffness matrix $\overline{\mathbf{K}}$ there is an eigenvector $\overline{\mathbf{Q}}$. For a system described by Eq. (2.2), it is possible to determine a set of parameters for the i-th mode, such as natural frequencies ω_i, damping ratios ξ_i, and mode shapes $\overline{\mathbf{P}}_i$. When the system is proportionally damped, the relationship $\overline{\mathbf{Q}}_i = \overline{\mathbf{P}}_i$ holds. For non-proportionally damped systems, $\overline{\mathbf{Q}}_i \neq \overline{\mathbf{P}}_i$ and the following relationship exists [11]:

$$\xi_i + j\zeta_i = \frac{1}{2\omega_i} \frac{\overline{\mathbf{Q}}_i^{\mathrm{T}} \overline{\mathbf{C}\mathbf{P}}_i}{\overline{\mathbf{Q}}_i^{\mathrm{T}} \overline{\mathbf{P}}_i}, \tag{2.3}$$

where $j = \sqrt{-1}$. The real part of the right-hand side of Eq. (2.3) is the traditional damping ratio ξ_i, while the complex part of the right-hand side of Eq. (2.3) is the energy transfer ratio ζ_i.

For proportionally damped systems, the vector $\overline{\mathbf{P}}_i$ is real and $\overline{\mathbf{P}}_i = \overline{\mathbf{Q}}_i$, and therefore $\zeta_i = 0$ which indicates the absence of energy transfer between vibration mode shapes. For non-proportionally damped systems, the vector $\overline{\mathbf{P}}_i$ is complex and $\zeta_i \neq 0$, which means that there is energy transfer between the vibration modes.

As can be seen from Eq. (2.3), in order to determine the ETR, it is necessary to know the damping matrix of the system under analysis. If a model of the system under study is available during experimental testing, the damping matrix built for the computational model can be used. As reported in [16], it is also possible to determine the ETR from experimental data alone. In the present analyses, the ETR will be determined using the damping matrix specified for the computational beam model described later in this paper.

More detailed information on the ETR can be found in [11, 15, 16].

3. Experimental studies

The composite beam that was tested consisted of an IPE 160 steel I-beam (S235JRG2 steel) with a span of 3200 mm, a reinforced concrete slab 600 mm wide and 60 mm thick (C30/37 concrete), and perfobond shear connectors (Fig. 1).

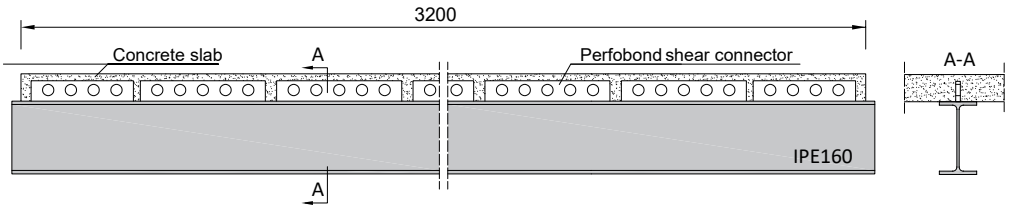

FIG. 1. Tested composite beam.

The analyses were carried out for a free-free beam. In this way, the influence of boundary conditions on the results was eliminated. In order to minimize the influence of support flexibility on the measurement results, the beam was suspended by means of flexible steel cables from a steel frame.

Fifty-two measuring points were located on the beam – 39 points on the upper surface of the concrete slab (visible in Fig. 2a) and 13 measuring points

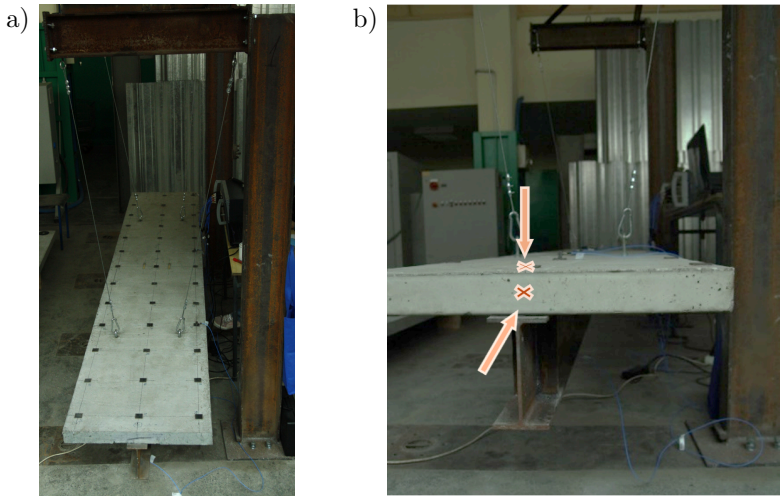

FIG. 2. View of the tested beam (a) and excitation points (b).

on the lower surface of the steel I-beam. An impulse test was carried out using a modal hammer. Accelerations were measured as system responses using piezoelectric acceleration sensors. The LMS SCADAS III signal analyser and LMS Test software (Lab 13A, 2015) were used for the tests. The beam was tested twice – with a force pulse applied to one end of the beam, once along the beam axis and once perpendicular to the surface of the concrete slabs (Fig. 2b). It should be clarified that forcing the beam with a force pulse along the beam axis was intended to determine the fundamental frequency of axial vibration, which was later used to identify the beam model parameters in subsequent stages of the study.

It should be mentioned that, although the beam was surveyed at 52 measurement points, only the measurement points located along the midplane of the beam – the measurement points located on the steel I-beam and the points on the concrete slab directly above the I-beam – were considered for further analysis. Data from points at the edges of the concrete slab were therefore not used. This approach was adopted to enable the construction of a single-plane model of the beam. The measurement points included in the analyses (along with a description of the sensor numbering used) are shown in the Fig. 3.

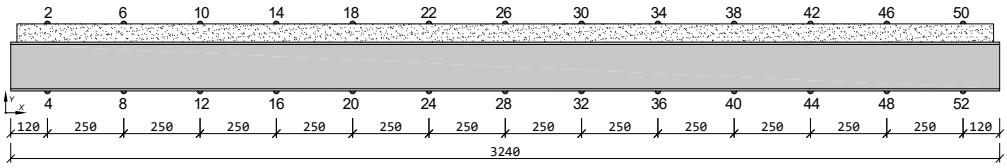

FIG. 3. View of the analysed beam plane with sensor numbering.

Table 1 lists the natural frequencies and the corresponding values of the damping ratios for the first five flexural mode shapes. The initial axial vibration frequency was $f_{1,a,\mathrm{exp}} = 579.66\,\mathrm{Hz}$.

Table 1. Natural frequencies and corresponding damping ratios.

$f_{i,\mathrm{exp}}$ [Hz] →	75.06	178.90	287.98	389.31	489.70
$\xi_{i,\mathrm{exp}}$ [%] →	0.127	0.173	0.284	0.500	0.753

More detailed information on the tested beam is available in [21].

4. Mathematical model of a composite beam

The rigid finite element method (RFEM) [22] was used to model the composite beam. This method has previously been used to model steel-concrete beams with good results [23]. While discrete modelling of structures using RFEM is less well known than the conventional FEM, it provides results that are in good agreement with FEM [24]. The main advantage of RFEM is the significantly smaller number of degrees of freedom of the system compared to the FEM method, which enables easier and faster calculations. The core idea of RFEM is to divide the system into rigid bodies, called rigid finite elements (RFEs), which are connected by spring-damping elements (SDEs). A single-plane model was constructed for the beam (Fig. 4). The steel and concrete parts were modelled separately. In the steel section, the RFEs were connected by not a single, but by three SDEs – located at the axis of the top flange, web and bottom flange. This approach made it possible to introduce damage to the bottom flange of the beam into the model. The use of RFEM in composite beams can also be found in [24, 25].

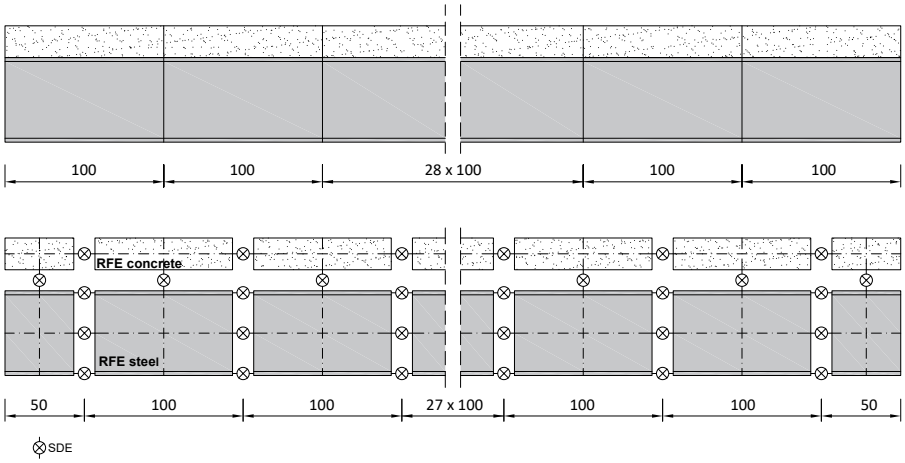

Fig. 4. RFE model of the composite beam.

For the description of the model, the parameters for the steel I-section and the concrete slab were adopted according to Table 2, where E_s is the Young modulus of steel, $\upsilon_{s/c}$ is the Poisson ratio for steel/concrete slab, G_s is the shear modulus of steel (Kirchhoff modulus for steel), $\rho_{s/c}$ is the density of steel/concrete, $A_{s,f}/A_{s,w}$ is the cross-sectional area of the beam flange/web, and h_c is the thickness of the reinforced concrete slab.

Table 2. Beam model parameters.

Steel I-beam						Concrete slab		
E_s [N/m^2]	υ_s	G_s [N/m^2]	ρ_s [kg/m^3]	$A_{s,f}$ [m^2]	$A_{s,w}$ [m^2]	υ_c	ρ_c [kg/m^3]	h_c [cm]
$210 \cdot 10^9$	0.3	$80.77 \cdot 10^9$	7850	$6.07 \cdot 10^{-4}$	$7.95 \cdot 10^{-4}$	0.2	2458.8	6.03

The three missing parameters describing the stiffness properties of the beam: the Young modulus that considers the reinforcement E_c, and the stiffness of the connection in both directions (X and Y) K_X and K_Y were determined based on parametric identification. The identification criteria included the best fit of the first five flexural natural frequencies and the overall fit of the first axial natural frequency obtained from experimental and numerical analyses. Table 3 contains identified beam stiffness parameters and flexural vibration frequency values of the beam determined for the model.

Table 3. Identified beam stiffness parameters and beam flexural vibration frequencies.

E_c [GPa]	K_X [N/m]	K_Y [N/m]	$f_{1,\text{num}}$ [Hz]	$f_{2,\text{num}}$ [Hz]	$f_{3,\text{num}}$ [Hz]	$f_{4,\text{num}}$ [Hz]	$f_{5,\text{num}}$ [Hz]
28.7	$8.10 \cdot 10^8$	$2.78 \cdot 10^8$	75.79	177.63	287.99	391.49	487.97

More detailed information on the model and the identification of stiffness properties is available in [21].

In order to determine the damping properties of the beam, the material loss factor μ was used. The loss factor is a characteristic of the material from which a component is made. For multi-material structures, it is a function of the damping of the individual constituent materials from which the structure is made. For the composite beam under consideration, three loss factors had to be considered – for the steel, the concrete, and the connection. All three components affect the damping properties of the beam.

For the Kelvin–Voight damping model, the relationship between the damping coefficients and stiffness coefficients for the k-th spring-damping element (SDE) is expressed as follows [26]:

$$c^k = \frac{\eta}{\omega} k^{(k)}. \tag{4.1}$$

For the beam tests, the loss factor for steel was assumed to have a constant value of $\eta_s = 4 \cdot 10^{-4}$. In [27], it can be found that the loss factor for steel is $\eta_s = (2 \div 6) \cdot 10^{-4}$. As the concrete slab is reinforced, its loss factor is also influenced by the reinforcement used. Therefore, the loss factors for the concrete slab and the connection were determined by parametric identification. It consisted of fitting frequency response functions (FRFs) obtained from numerical model to those from the experimental studies. The analyses included the first three resonances of the flexural mode shapes and one axial mode for four selected measurement points. The choice of measurement points adopted for identification was dictated by their locations on the beam.

Based on this identification, the values of the loss factors were obtained: $\eta_c = 70 \cdot 10^{-4}$ for the concrete slab, and $\eta_{\text{conn}} = 418 \cdot 10^{-4}$ for the connection. Figure 5 and Fig. 6 show the FRFs obtained during the experimental tests and those from the model after identification.

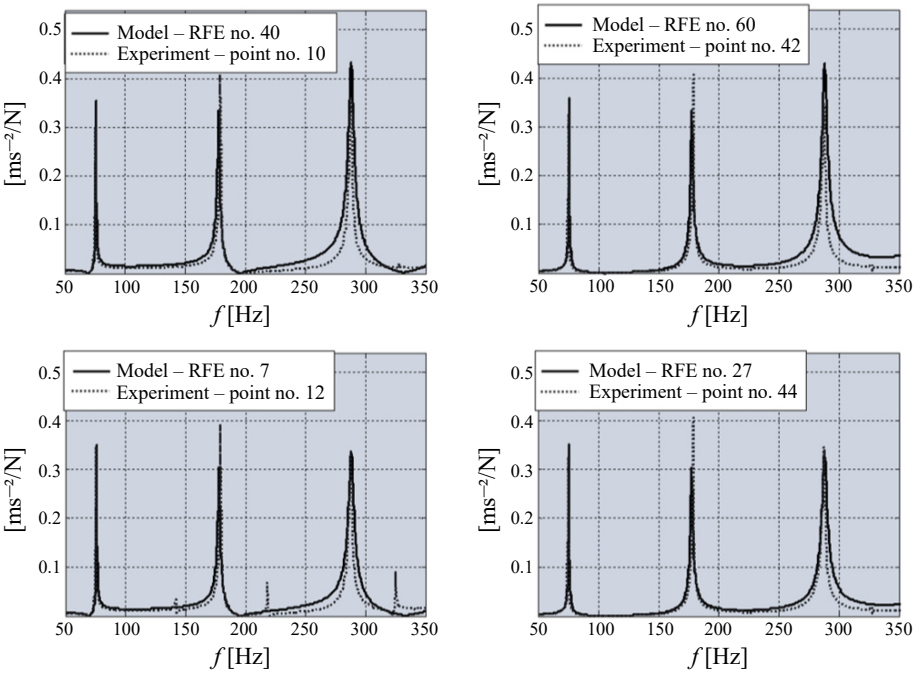

FIG. 5. FRF obtained from experimental tests and from the model with excitation in the Y-axis direction.

In order to check the compatibility of the model with the experimental results, the modal assurance criterion (MAC) values were determined for the first five determined modes of flexural vibration. As the MAC values for the fourth and fifth modes of vibration were below 0.8, these modes of vibration were not taken into account in further analyses.

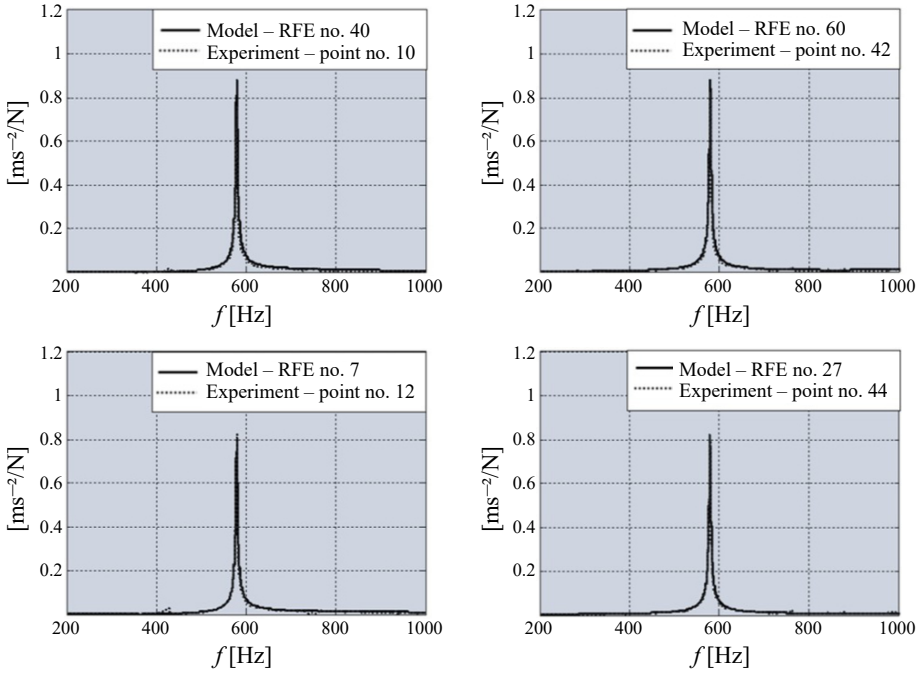

FIG. 6. FRF obtained from experimental tests and from the model with excitation in the X-axis direction.

5. BEAM DAMAGE SIMULATION

Damage was introduced to the I-section steel beam by incising the bottom flange over its full width (Fig. 7).

FIG. 7. Damage to the bottom flange.

The damage was located at two points – indicated in Fig. 8 by symbols A and B. In the first stage, a flange incision was introduced at point 1 (damage D1). In the next stage, a flange incision was introduced at point 2 (damage D2).

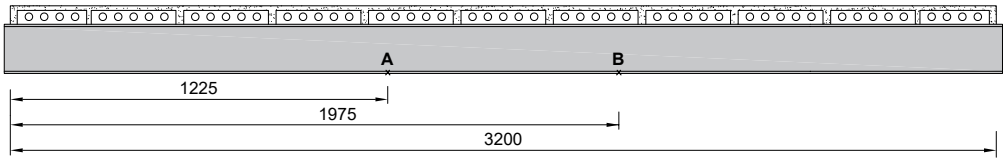

FIG. 8. Locations of damage.

The numerical simulation of the damage consisted of changing the elastic properties (the beam flange cross-sectional area $A_{s,f} = 0$ and moment of inertia of the flange about the Z-axis of the cross-section $I_{z,s,f} = 0$) of the corresponding SDEs modelling the bottom flange. These properties were set: a) for damage D1 at location 1, and b) for damage D2 at locations 1 and 2, respectively.

6. RESEARCH RESULTS

Changes in modal parameters as a result of damage were determined using the index Δ_i:

$$\Delta_i = \left| \frac{x_{i,d} - x_{i,u}}{x_{i,u}} \right|, \tag{6.1}$$

where $x_{i,d}$ and $x_{i,u}$ denote the modal parameter in the damaged and undamaged states, respectively.

6.1. Damping ratio

The values of the damping ratio and their changes due to the introduced damages D1 and D2, presented separately for experimental test results and the numerical model, are presented in Table 4. The condition of the beam without damage is denoted as D0. Changes in the damping ratio also illustrated graphically in Fig. 9.

TABLE 4. Damping ratios before and after damage.

	Beam state									
	Experimental test					Numerical model				
	D0	D1		D2		D0	D1		D2	
i	$\xi_{i,\text{exp}}$ [%]	$\xi_{i,\text{exp}}$ [%]	Δ_i [%]	$\xi_{i,\text{exp}}$ [%]	Δ_i [%]	$\xi_{i,\text{num}}$ [%]	$\xi_{i,\text{num}}$ [%]	Δ_i [%]	$\xi_{i,\text{num}}$ [%]	Δ_i [%]
1_{flex}	0.127	0.137	8.0	0.137	7.6	0.236	0.237	0.7	0.238	1.0
2_{flex}	0.173	0.186	7.9	0.265	53.5	0.473	0.467	1.1	0.462	2.2
3_{flex}	0.284	0.309	8.7	0.296	4.0	0.683	0.681	0.3	0.679	0.6

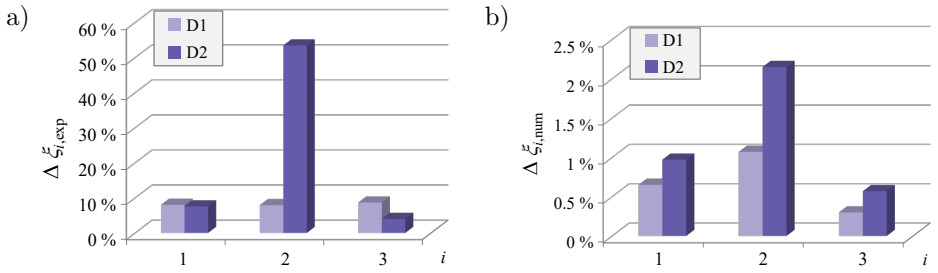

FIG. 9. Changes in damping ratio before and after damage:
a) experimental test, b) numerical model.

As presented, small changes in the modal damping ratio were observed as a result of the numerical damage simulation. The largest changes in the numerical analyses were only 2.2 %. Higher sensitivity was obtained during the experiment, with changes of a few percent, except for one value reaching 53.5 %. It can also be observed that the modal damping ratios determined from the numerical model were higher than those obtained during experimental tests. The maximum changes in damping ratio appeared to coincide for both the experiment and numerical analyses, occurring for the second mode shape at damage D2.

6.2. ETR

The ETR was determined from Eq. (2.3). A prerequisite for the determination of this ratio according to Eq. (2.3) is knowledge of the damping matrix $\overline{\mathbf{C}}$. It should be noted that the $\overline{\mathbf{C}}$ matrix determined for the numerical model was also used to determine the ETR from experimental tests. The values of the ETR and their changes due to the introduced damages D1 and D2 are shown in Table 5. The condition of the beam without damage is denoted as D0. Changes in the ETR are also graphically illustrated in Fig. 10.

TABLE 5. Changes in ETR index before and after damage.

	Beam state									
	Experimental test					Numerical model				
	D0	D1		D2		D0	D1		D2	
i	$\zeta_{i,\mathrm{exp}}$ [‰]	$\zeta_{i,\mathrm{exp}}$ [‰]	Δ_i [%]	$\zeta_{i,\mathrm{exp}}$ [‰]	Δ_i [%]	$\zeta_{i,\mathrm{num}}$ [‰]	$\zeta_{i,\mathrm{num}}$ [‰]	Δ_i [%]	$\zeta_{i,\mathrm{num}}$ [‰]	Δ_i [%]
1_{flex}	5.420	2.980	45.0	3.610	33.4	0.050	0.048	4.3	0.046	8.2
2_{flex}	1.712	0.587	65.7	1.011	40.9	0.108	0.106	2.3	0.103	5.0
3_{flex}	1.584	0.696	56.1	0.529	66.6	0.138	0.138	0.3	0.138	0.5

As shown, large changes in the ETR as a result of the damage introduced were observed in the experimental tests – with all changes in the range of tens

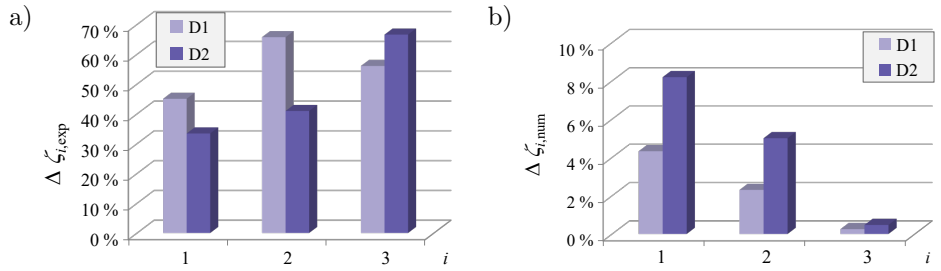

Fig. 10. Changes in ETR before and after damage: a) experimental test, b) numerical model.

of percent. These are significantly larger values than those obtained for the damping ratio. Analysing the results of numerical tests – a few percent changes in ETR were obtained, which still turned out to be larger than those obtained for the damping ratio (except for for the third mode shape, where these changes were at a similar level).

7. Conclusions

This paper aimed to assess the sensitivity of modal parameters characterising damping in non-proportionally damped systems. Damage was introduced to the bottom flange of a steel I-beam in a steel-concrete composite beam. The results obtained from experimental tests and from the numerical model were analysed. The sensitivity of the damage introduced was assessed for two damping parameters – the damping ratio and the ETR. As a result of the experimental tests and numerical analyses for the composite beam, a little sensitivity of the damping ratio to damage introduced into the beam was observed. The damping ratio is therefore not a good indicator of damage for the beam under analysis. Regarding the ETR – it was observed that the ETR was more sensitive to introduced damage than the damping ratio. Additionally, the ETR was more responsive to changes in the composite beam than the damping ratio. This suggests that perhaps the ETR could be used as a damage detection tool. It should be mentioned that, although this paper analysed one type of damage in a single composite beam, the method based on variations in ETR due to damage can be applied to different structures using different numerical modelling techniques. Studies by other researchers, in which ETR changes were analysed, were performed on composite bridge models [15–17], showing that the method can be applied to a variety of structures. To estimate the energy transfer for a vibration mode, it is necessary to know the frequency, mode shape, and damping matrix. Consequently, various numerical modelling techniques can be used to build the computational model. The determination of the ETR for non-proportionally damped systems is based on changes in the complex mode shape

of vibration. In order to avoid errors in phase determination, the method requires a great deal of care when taking measurements. The presence of uncontrolled measurement noise can affect the results obtained. Nevertheless, the continuous development of technology provides new opportunities. New technologies are also being introduced into SHM for engineering structures, allowing more precise measurements. Perhaps, the ETR could be used as a potential tool for damage detection.

Fundings

The project has been financed by the National Science Centre.

Conflict of interest

The author declares that she has no known competing financial interests or personal relationships that could have appeared to influence the work reported in this paper.

Author's contribution

The author reviewed and approved the final manuscript.

Acknowledgments

The manuscript was prepared as a conference paper for the 31st Conference on Vibrations in Physical and Technical Systems, October 16–18, 2024, Poznań, Poland.

References

1. Choo J.F., Choi Y.C., Choi W.C., Yoo S.W., Behavioral characteristics of hybrid girders according to type of steel–concrete connection, *Archives of Civil and Mechanical Engineering*, **19**(1): 47–62, 2019, https://doi.org/10.1016/j.acme.2018.08.008.
2. Haque M.N., Maki T., Experimental study on time-dependent deformation of hybrid steel–PRC girder with headed stud shear connections under sustained loading, *Structures*, **22**: 327–340, 2019, https://doi.org/10.1016/j.istruc.2019.09.004.
3. Kim S.E., Nguyen H.T., Evaluation of the connection efficiency of hybrid steel-concrete girder using finite element approach, *International Journal of Mechanical Sciences*, **61**(1): 8–23, 2012, https://doi.org/10.1016/j.ijmecsci.2012.04.008.
4. Ghanim G., Baldawi W.S., Ali A.A., A review of composite steel plate girders with corrugated webs, *Engineering and Technology Journal*, **39**(12): 1927–1938, 2021, https://doi.org/10.30684/etj.v39i12.2193.

5. Chen Y., Dong J., Xu T., Composite box girder with corrugated steel webs and trusses – A new type of bridge structure, *Engineering Structures*, **166**: 354–362, 2018, https://doi.org/10.1016/j.engstruct.2018.03.047.

6. Pardeshi R.T., Patil Y.D., Review of various shear connectors in composite structures, *Advanced Steel Construction*, **17**(4): 394–402, 2021, https://doi.org/10.18057/IJASC.2021.17.4.8.

7. Sohn H., Farrar C.R., Hemez F.M., Czarnecki J.J., Shunk D.D., Stinemates D.W., Nadler B.R., *A review of structural health monitoring literature*, Los Alamos National Laboratory Report, LA-13976-MS, pp. 1996–2001, 2003.

8. Montalvão D., Maia N.M.M., Ribeiro A.M.R., A review of vibration-based structural health monitoring with special emphasis on composite materials, *Shock and Vibration Digest*, **38**(4): 295–324, 2006, https://doi.org/10.1177/0583102406065898.

9. Das S., Saha P., Patro S.K., Vibration-based damage detection techniques used for health monitoring of structures: A review, *Journal of Civil Structural Health Monitoring*, **6**(3): 477–507, 2016, https://doi.org/10.1007/s13349-016-0168-5.

10. Yang Y., Zhang Y., Tan X., Review on vibration-based structural health monitoring techniques and technical codes, *Symmetry*, **13**(11): 1–18, 2021, https://doi.org/10.3390/sym13111998.

11. Liang Z., Lee G.C., *Damping of structures: Part 1 – Theory of complex damping*, National Center for Earthquake Engineering Research, Technical Report NCEER-91-0004, State University of New York at Buffalo, 1991.

12. Caughey T.K., O'Kelly M.E.J., Classical normal modes in damped linear dynamic systems, *Journal of Applied Mechanics*, **32**(3): 583–588, 1965, https://doi.org/10.1115/1.3627262.

13. Ewins D.J., *Modal Testing: Theory, Practice, and Application*, 2nd ed., Research Studies Press, England, 2000.

14. Wenzel H., Pichler D., *Ambient Vibration Monitoring*, John Wiley & Sons, England, 2005.

15. Zong Z.H., Wang T.L., Structural damage identification by using energy transfer ratio, [in:] *Conference Proceedings, 21st IMAC Conference and Exposition (IMAC XXI), A Conference and Exposition on Structural Dynamics*, Kissimmee, Florida, 2003.

16. Wang T.L., Zong Z., *Improvement of evaluation method for existing highway bridges*, Technical Report FL/DOT/RMC/6672-818, Florida Department of Transportation, USA, 2002.

17. Lee G.C., Liang Z., Development of a bridge monitoring system, [in:] *Proceedings of the 2nd International Workshop on Structural Health Monitoring*, pp. 349–358, Stanford University, California, 1999.

18. Wróblewski T., Jarosińska M., Berczyński S., Application of ETR for diagnosis of damage in steel-concrete composite beams, *Journal of Theoretical and Applied Mechanics*, **49**(1): 51–70, 2011.

19. Wróblewski T., Jarosińska M., Berczyński S., Damage location in steel-concrete composite beams using energy transfer ratio (ETR), *Journal of Theoretical and Applied Mechanics*, **51**(1): 91–103, 2013.

20. Wróblewski T., Jarosińska M., Abramowicz M., Berczyński S., Experimental validation of the use of energy transfer ratio (ETR) for damage diagnosis of steel-concrete composite beams, *Journal of Theoretical and Applied Mechanics,* **55**(1): 241–252, 2017, https://doi.org/10.15632/jtam-pl.55.1.241.

21. Jarosińska M., Wróblewski T., Identification of damage to a steel I-beam based on changes in frequency and curvature of the mode shape in a steel-concrete composite beam, *Archives of Civil Engineering*, **71**(2): 575–590, https://doi.org/10.24425/ace.2025.154138.

22. Kruszewski J., Gawroński W., Wittbrodt E., Najbar F., Grabowski S., *The Rigid Finite Element Method* [in Polish: *Metoda Sztywnych Elementów Skończonych*], Arkady, Warszawa, 1975.

23. Berczyński S., Wróblewski T., Experimental verification of natural vibration models of steel-concrete composite beams, *Journal of Vibration and Control*, **16**(14): 2057–2081, 2010, https://doi.org/10.1177/1077546309350552.

24. Abramowicz M., Pełka-Sawenko A., Comparison of the finite element method and rigid finite element method during dynamic calculations of steel–concrete composite beams based on experimental results, *Materials*, **17**(24): 6081, 2024, https://doi.org/10.3390/ma17246081.

25. Abramowicz M., Berczyński S., Wróblewski T., Modelling and parameter identification of steel–concrete composite beams in 3D rigid finite element method, *Archives of Civil and Mechanical Engineering*, **20**: 103, 2020, https://doi.org/10.1007/s43452-020-00100-7.

26. Kruszewski J., Sawiak S., Wittbrodt E., *Computer-aided Design CAD/CAM, The Rigid Finite Element Method in Dynamics of Structures* [in Polish: *Wspomaganie Komputerowe CAD/CAM, Metoda Sztywnych Elementów Skończonych w Dynamice Konstrukcji*], Wydawnictwa Naukowo-Techniczne, Warszawa, 1999.

27. Rao S.S., *Mechanical Vibrations*, 5th ed., Prentice Hall, 2011.

Received December 18, 2024; revised May 31, 2025; accepted June 5, 2025; version of record March 9, 2026; published issue March 30, 2026.